Contents lists available at ScienceDirect

Applied Catalysis B: Environmental

journal homepage: www.elsevier.com/locate/apcatb

Hydrogen generation by irradiation of commercial CuO + TiO$_2$ mixtures at solar pilot plant scale and in presence of organic electron donors

M.I. Maldonado[a,b,*], E. Saggioro[c], J. Peral[d,**], E. Rodríguez-Castellón[e], J. Jiménez-Jiménez[e], S. Malato[a,b]

[a] Plataforma Solar de Almería (CIEMAT), Carretera de Senés, km 4, 04200, Tabernas, Almería, Spain
[b] CIESOL, Centro de Investigación en Energía Solar, Centro Mixto Universidad de Almería-CIEMAT, 04120 Almería, Spain
[c] Department of Sanitation and Environmental Health, National School of Public Health, Oswaldo Cruz Foundation, Rio de Janeiro, Brazil
[d] Departament de Química, Universitat Autònoma de Barcelona, Edifici Cn, 08193, Bellaterra, Cerdanyola del Vallés, Spain
[e] Department of Inorganic Chemistry, Universidad de Málaga, Málaga, Spain

ARTICLE INFO

ABSTRACT

A CuO + TiO$_2$ mixture, based on two commercial and well characterized CuO and TiO$_2$ photocatalyst, has been used to produce hydrogen by solar light irradiation and in presence of different organic compounds (methanol, glycerol, formic acid, and the components of a wastewater coming from the biodiesel industry) acting as sacrificial electron donors. The experiments have been conducted at Plataforma Solar de Almería (PSA, south of Spain) with a pilot plant scale reactor using a CPC (compound parabolic collector) configuration. The tested system has shown similar hydrogen generation capacity and energy efficiency than more expensive ones based on the use of noble metal/photocatalyst composites. Formic acid has shown to be the most effective electron donor, although very close amounts of hydrogen are also produced with glycerol, and this is found as a waste compound released in large quantities at the biodiesel industry wastewaters. As seen in previous similar studies, the increase of solution conductivity hampers the hydrogen generation, and a slightly basic solution pH (pH ≈ 9) gives the best reaction conditions. Finally, the composite can be recovered and successfully reused giving the ensuing and sustained generation of H$_2$ while removing more than 50% of TOC.

1. Introduction

The need for abundant and clean sources of new fluid fuels is imperative in order to reduce the planetary climate change produced by the combustion of fossil fuels, and to avoid the world economical crash expected after the reserves of those fuels are exhausted. Hydrogen is one of the most promising renewable alternatives to fossil fuels. It can be produced from renewable resources and can be safely stored [1,2], and it is considered an ideal energy carrier as it can store 3 times as much energy as conventional natural gas, while its combustion is environmentally friendly [3]. Nowadays, the main large scale H$_2$ production comes from the steam reforming of methane, a process that involves the consumption of fossil fuel energy, being this the reason why much research is devoted to find alternative technologies for producing hydrogen in a renewable way [4]. One particularly appealing possibility aroused from the 1972 reported photoelectrochemical hydrogen production of Fujishima and Honda [5], and the

many papers dealing with the generation of that gas from water by using semiconductor photocatalysts and light that have been published afterwards [6–9]. Although, in principle, the efficiency of the direct water splitting by heterogeneous photocatalysis is rather low, hydrogen generation can be notably increased in presence of aqueous sacrificial agents (organic electron donors) [10–13]. Aqueous pollutants can play the role of those organic sacrificial agents and, consequently, simultaneous hydrogen production and pollutant removal can be obtained. The general chemical reaction for such a process can be summarized as follows:

$$C_xH_yO_z + (2x - z)H_2O \xrightarrow[h\nu \geq E_g]{photocatalyst} xCO_2 + \left(2x - z + \frac{y}{2}\right)H_2 \quad (1)$$
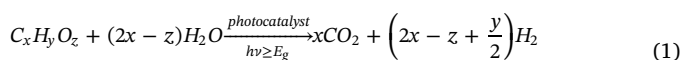
a reaction that has been referred to as photoreforming.

By far, the most used material in heterogeneous photocatalysis has been titanium dioxide (TiO$_2$), due to its high chemical stability, nontoxic character, strong oxidizing power and low price [14–18].

* Corresponding author at: Plataforma Solar de Almería (CIEMAT), Carretera de Senés, km 4, 04200, Tabernas, Almería, Spain.
** Corresponding author.
E-mail addresses: mmaldonado@psa.es (M.I. Maldonado), jose.peral@uab.cat (J. Peral).

Nevertheless, the band gap of TiO_2 is too large, leaving this material useless for visible light activation. Also, the electron-hole recombination in TiO_2 is very fast, giving charge lifetimes that are just too short living for adequate reaction, something that limits the efficiency of the material as catalyst. The alternative use of composite materials based on TiO_2 has been explored because the existence of the interface between the components of the composite can improve charge separation and reduce electron-hole recombination. Deposition of noble metal nanoparticles (Pt or Au) on the TiO_2 surface has been one appealing possibility because noble metals efficiently trap TiO_2 conduction band electrons [19]. However, noble metals are just too expensive to be considered as feasible alternative from a practical point of view. Another possibility has been the synthesis of composites between TiO_2 and other semiconducting materials (oxides, chalcogenides, etc.) [20]. Apart from obtaining an efficient charge separation, the existence of other composite material able to absorb light in the visible range of the spectrum widens the fraction of solar light that can be used in the process. In this sense, photoactive CuO phases have been used as viable components of TiO_2 composites because they are easy to prepare, cheap, stable enough, and have a strong absorption of visible light photons. In particular, production of H_2 from ethanol/water solutions and visible light irradiation of a CuO/TiO_2 composite has been reported by Xu and Sun [21]. Those authors found that their composite produced hydrogen generation rates significantly higher than the ones reported with some noble metal (Pt and Pd) loaded TiO_2. The role of the CuO crystallites on the photocatalytic hydrogen generation with the CuO/TiO_2 composite was also studied in detail by Chen et al. [22]. Particularly interesting is the contribution by Kum et al. [23]. Those authors have being able to produce large amounts of H_2 with the mixing in solution of commercial CuO and TiO_2 particles, showing that no continuous and stable contact between particles is always needed to obtain charge transfer and separation and to improve the photocatalytic performance. Apart from the above mentioned works several other articles highlighting the beneficial role of the CuO/TiO_2 composites for photocatalytic hydrogen production can be found elsewhere [14,24–26].

In addition to photocatalyst improvement the optimization of the process from a reactor design point of view is crucial in order to make the photocatalytic hydrogen production a feasible procedure. Some authors have recently reported that the cost of direct solar hydrogen production from water by photoreforming can be below $2.90 per kilogram of hydrogen after compression and distribution if technical progress is made to achieve an optimum photocatalyst and with appropriate plant-scale engineering [27,28]. So far, the poor quantum efficiencies reported and the scarcity of scaling-up studies make the practical industrial application of this technology almost non-existent. In this sense, a limited number of works about hydrogen generation via solar heterogeneous photocatalysis at pilot-plant scale have been reported so far [15,16,29–32]. Baniasadi et al. [29] analysed the exergy efficiency, exergy destruction, environmental impact and sustainability index of a continuous production of hydrogen at a pilot-plant scale. Linkous et al. [30] developed a reactor configuration for photochemical hydrogen production from semiconductor slurries containing H_2S. Platinized CdS was utilized as the photocatalytic material. Jing et al. [31] designed a Compound Parabolic Concentrator (CPC) for solar photocatalytic hydrogen production and they reported some preliminary results using CdS as photocatalyst but they failed to report the sacrificial agent used. Finally, Villa et al. [15], Arzate-Salgado et al. [16], and Maldonado et al. [32] have reported photocatalytic hydrogen generation experiments using N-doped TiO_2, CdS/ZnS, Au/TiO_2 and Cu/TiO_2 composite catalysts in the same pilot plant scale CPC photoreactor employed in the present work, and they have shown that in all cases the system could work by using real wastewaters as source of sacrificial organic molecules.

In an effort to produce hydrogen with a solar heterogeneous photocatalytic system that has real possibilities for practical application we have chosen to explore here the potential of the mixture of commercial nanoparticles of CuO and TiO_2 reported by Kum et al. [23] working in the pilot plant scale CPC photoreactor located at PSA [15,16,32]. The main objective is to evaluate the solar large scale performance of the cheap, simple (no need for the synthesis of an stable composite interface), and well characterized commercial nanoparticle mixture that has been able to produce remarkable quantities of H_2 at laboratory scale and, also, to use different sacrificial electron donor species, in particular some of them contained in real wastewaters. Special attention has also been given to the influence of pH on the reaction efficiencies. The CPC used in this study, designed with a concentration ratio of 1 (no concentration of solar radiation, only light reflexion towards glass tube), is the best option to capture both the direct and diffuse solar radiation. Besides, it generally exhibits high optical and quantum efficiencies, and it has a low-cost [33].

2. Experimental

2.1. Reagents

P25 TiO_2 with on average diameter of 25 nm was obtained from Degussa, Germany. Commercialized CuO nanoparticles from Sigma Aldrich were used. The average size of the CuO nanoparticles was 50 nm. The rest of reagents used in this work were of analytical grade. High purity N_2 (99.9992%) was used to provide an O_2 free atmosphere. A commercial gas mixture of 1000 ppmv of H_2 in N_2 was used for GC calibration. Demineralised water and tap water from PSA (see Table 1 for main chemical composition) were used to prepare aqueous solutions. Table 1 also shows the main physicochemical features of the real wastewater generated in a large scale biodiesel production facility.

2.2. Catalysts characterisation

X-ray powder diffraction patterns (XRPD) of catalysts were recorded on a PAN analytical X'Pert diffractometer. Powder patterns were recorded between 5 and 80° in 2θ, with a step size of 0.017° (2θ) and an equivalent counting time of ∼60 s/step, in Bragg-Brentano reflection configuration by using a Ge (111) primary monochromator (Cu Kα1) and the X'Celerator detector. UV–vis-NIR diffuse reflectance spectra of powder samples were recorded, at room temperature, in the range 200–1400 nm, with a spectrometer model Agilent Cary 7000 and a diffuse reflectance accessory of 150 mm of internal diameter. XPS measurements were carried on a Physical Electronics spectrometer model Versa Probe II with monochromatic X-ray Al Kα radiation (100 μm, 100 W, 20 kV, 1486.6 eV) and a dual beam ncharge neutralizer. The energy scale was calibrated using Cu $2p_{3/2}$, Ag $3d_{5/2}$, and Au $4f_{7/2}$ photoelectron lines at 932.7, 368.2 and 84.0 eV, respectively. Under a constant pass energy mode at 23.5 eV, the Au $4f_{7/2}$ line was recorded with 0.73 eV FWHM at a binding energy (BE) of 84.0 eV. Recorded spectra were always fitted using Gauss–Lorentz curves. Atomic percentages of the characteristic surface elements were determined taking into account the corresponding area sensitivity factor

Table 1

Main physicochemical features of the demineralized and tap waters of PSA, and the biodiesel production wastewater (BDW) used in this work.

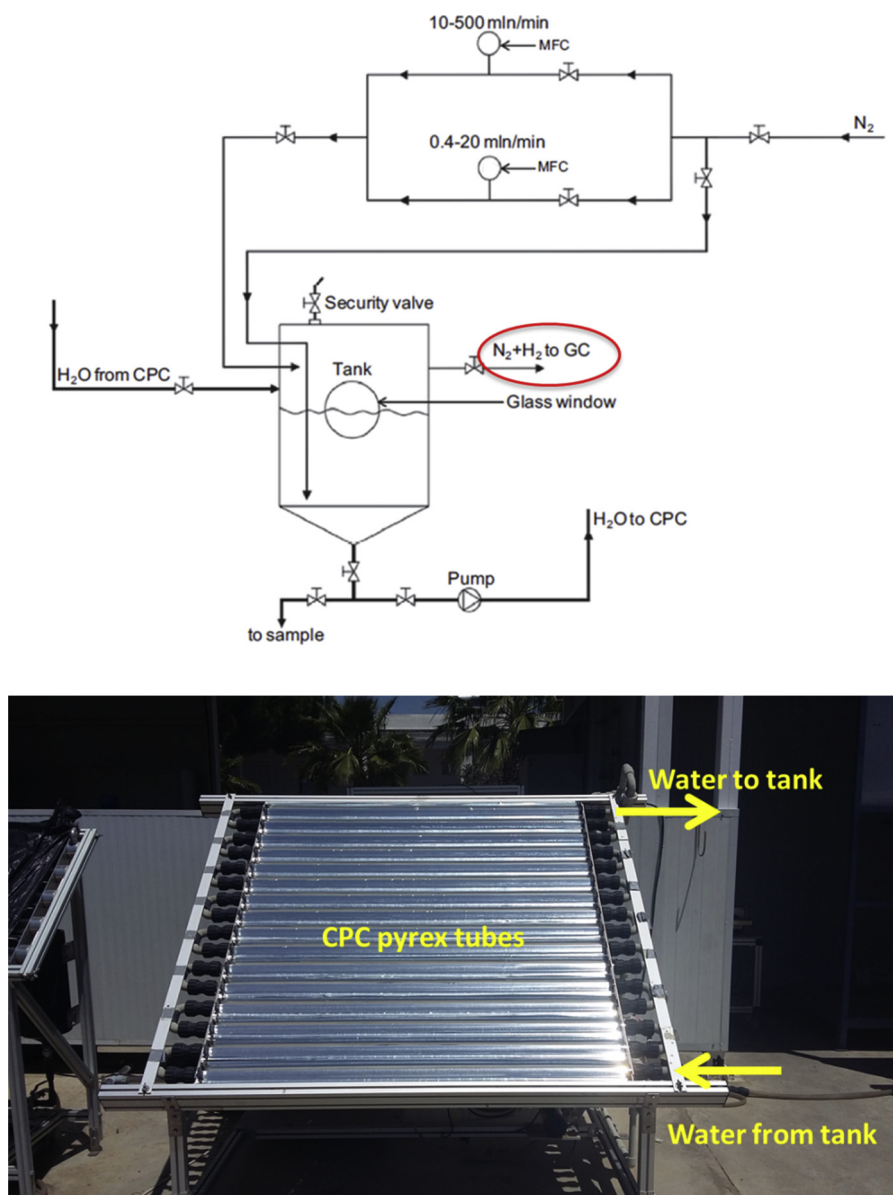|	PSA demineralized water	PSA tap water	Biodiesel wastewater (1:1000 dilution)
Conductivity (μS cm^{-1})	1.85	2500	120.7
DOC (mg L^{-1})	< 0.5	0.5	400-470
Cl$^-$ (mg L^{-1})	0.7-0.8	350	1.13-1.2
SO$_4^{-2}$ (mg L^{-1})	0.5	195	2.79-2.91
HCO$_3^-$/CO$_3^{2-}$ (mg L^{-1})	0.4	947	5.6
pH	5.0-6.0	7.5-8.0	6.0-6.5
Color	–	–	colorless

Fig. 1. Schematic drawing of CPC Pilot Plant (top) and picture of CPC photoreactor (down).

for the different measured spectral regions. Cu $2p$ and C $1s$ were first recorded with a short irradiation time (10 min) to avoid as much as possible the photoreduction of Cu^{2+}. Elemental chemical analysis was performed using a LECO CHNS932 analyzer. X-Ray Fluorescence measurements were carried out in a XRF by wavelength dispersion Advent XP of Thermo Fisher.

2.3. Photocatalytic runs

The pilot plant for photocatalytic hydrogen generation contained a closed stainless steel tank of 27 L of volume, fitted with gas and liquid inlet and outlet and a sampling port. Two parallel mass flow controllers could be used to control the desired N_2 gas flow into the reactor headspace during the reactor filling step. A centrifugal pump (PanWorld NH-100PX) with a flow rate of $20 \, L \, min^{-1}$ was used to recirculate the aqueous slurry from the tank to the tubes of the CPC. The photoreactor was composed of 16 Pyrex glass tubes (inner diameter 28.45 mm, outer diameter 32.0 mm, irradiated length 1401.0 mm) mounted on a fixed platform tilted 37° (local latitude), see Fig. 1. The total area and volume irradiated were $2.10 \, m^2$ and 14.25 L,

respectively. In all experiments, 25 L of solution were used (leaving 10.75 L in the dark distributed between the tank and the pumping pipelines). Empty headspace in the tank was around 21.0 L. Different sacrificial agents were tested: glycerol, methanol, formic acid (always at 0.05 M concentration), and the real industrial wastewater shown in Table 1.

At the beginning of each experiment the aqueous slurry prepared by mechanical mixing of the CuO and TiO_2 (1:10) powders (at $0.2 \, g \, L^{-1}$ of total concentration) was recirculated in the dark for 15 min to establish the adsorption–desorption equilibrium between organics and the photocatalyst. The oxygen present in the gas phase volume was pulled out with a pure N_2 flow that lasted until no more oxygen was detected. After that, the photoreactor was uncovered and the aqueous slurry was irradiated around 6 h. Gas samples were analysed at approximately 1 h intervals. The reactor head-space remained closed during the experiment (batch conditions).

Data obtained with solar radiation that lacks of steadiness and changes during the same day or during different days (time of day, year season, meteorological conditions, etc.) needs normalization in order to be useful for comparison of hydrogen generation between different

experiments (or even at different times of the same experiment). Eq. (2), where t_n is the sampling experimental time, W_s the average solar radiation measured by the radiometer (in $W \cdot m^{-2}$) during the period Δt_n, V_t is the total reactor volume, and A_i is the irradiated area of the reactor (CPC), can be used for such a normalization. Q_n ($kJ \cdot L^{-1}$) is the solar energy accumulated per reactor volume unit along the experiment, and it is used instead of the experimental time in order to take into account both experimental time and solar radiation fluctuation.

$$Q_n = Q_{n-1} + \Delta t_n \, W_s \frac{A_i}{V_t} \tag{2}$$

Solar radiation intensity was measured using a radiometer (KIPP& ZONNEN, CUV3 model) that provided data of the incident radiation corresponding to wavelengths below 400 nm (matching the absorption spectrum of TiO_2) and it was mounted on a platform at the same angle as the CPC. Data was recorded every minute in terms of $W \cdot m^{-2}$.

2.4. Analytical determinations

Hydrogen was analysed by using a gas micro-chromatograph (Agilent technologies 490) equipped with a TCD detector and a CP-MolSieve 5A column channel (10 m, with backflush and retention time stability). Pure N_2 was used as carrier gas. Organic degradation was quantified as dissolved organic carbon (DOC) by using a Shimadzu VCSH TOC analyser. Before DOC quantification, the samples were filtered (0.2 μm) with nylon filters.

3. Results and discussions

The crystalline phases of the fresh photocatalyst, prepared by mechanical mixing of CuO and TiO_2 (1:10), were identified by XRD (Fig. 2). TiO_2 anatase (JCPDS card No. 21-1272), TiO_2 rutile (JCPDS card No. 21-1276) and CuO tenorite (JCPDS card No. 01-089-2529) phases were detected and, as expected, anatase was the predominant phase.

Photocatalytic hydrogen generation of the CuO + TiO_2 mixtures prepared with the above described materials was carried out at the PSA pilot scale plant under solar irradiation. Different sacrificial electron donor species were tested. Two of those electron donors, formic acid and methanol, were chosen because of their low splitting energy demand (16.1 $kJ \, mol^{-1}$ for methanol and 32.9 $kJ \, mol^{-1}$ for formic acid compared to 237 $kJ \, mol^{-1}$ for water [34]) a fact that, along with the right position of their redox potential vs. the position of the photocatalyst valence band, makes them especially suited for the trapping of photogenerated valence band holes and the assistance of the photocatalytic process. Glycerol was also chosen because it is an organic molecule that has a low redox potential, having the additional
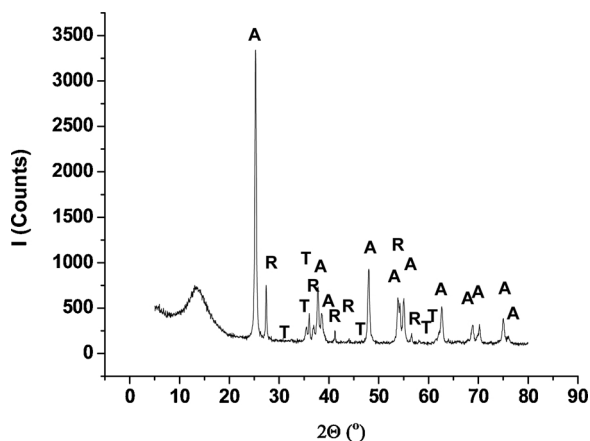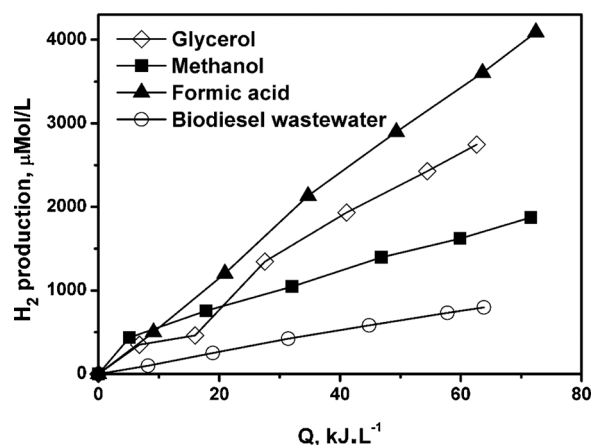
Fig. 3. Photocatalytic H_2 generation in presence of different sacrificial agents. Reaction conditions: $TiO_2 + CuO$ (10:1) $= 0.2 \, g.L^{-1}$, sacrificial agent conc. $= 0.05 \, M$, biodiesel wastewater TOC $= 1200 \, mg \, L^{-1}$, V $= 25 \, L$, and total irradiation time of 6 h. pH of the experiments (natural pH of the solutions): glycerol at pH 5–6, methanol at pH 6–7, formic acid at pH 2.5 and biodiesel wastewater at pH 6.

advantage of being very cheap because it is released in large quantities in the wastewaters produced by the biodiesel industry. The choice of their initial concentration (0.05 M) was aimed at simulate concentrations of organic compounds in real polluted waters. Initial pH values for methanol and glycerol solutions were around 6 while for formic acid was 2.5 (always the natural pH of the 0.05 M aqueous solutions of the three solutes). The pH values did not remain constant during the reactions time course, but with variations always below one pH unit. The same catalyst loading (0.2 $g \, L^{-1}$ of CuO + TiO_2) was used through the entire study. This loading has been described as the optimum for the CPC photoreactor of 32.0 mm outer diameter [35] and provided the best H_2 production in previous studies with other different catalytic systems at the same operational conditions (same location and reactor) [15,16,32]. A 1:10 CuO:TiO_2 weight ratio was kept in all experiment, based on the previous bench scale results of Kum et al. [23]. Fig. 3 shows the H_2 evolution vs. the amount of energy accumulated into the reactor for the three aqueous solutions. The figure also includes data of an experiment carried out with a wastewater of the biodiesel industry as source of electron donors. In that case TOC concentration was 1200 $mg \, L^{-1}$ and pH ≈ 6.

As can be seen, in all cases there is a remarkable generation of H_2. The capacity of each electron donor in terms of H_2 production follows the sequence formic acid > glycerol > methanol > biodiesel wastewater. This order can be justified by taking into account that formic acid has a smaller redox potential (higher tendency towards oxidation and release of electrons) than methanol and glycerol and, thus, its oxidation to CO_2 is rather easy, providing the electrons that are needed for the closure of the photocatalytic process. On the other hand, methanol and glycerol are two organic alcohols with similar redox potentials and, consequently, they provide H_2 production rates that are similar or, at least, in the same order of magnitude. Finally, although the biodiesel wastewater contains glycerol (according to the supplier information) the production of H_2 observed in that medium is far below the one observed for pure glycerol. In this case, as discussed later, a large content of inorganic salts and a large conductivity might be the cause for the lower reaction yield. The hydrogen production per amount of energy entering the reactor observed in Fig. 3 for formic acid is 55 $\mu mol \, kJ^{-1}$, and that is the best hydrogen production recorded in this work. A simple procedure that can provide a first idea of the capacity of this system for the photogeneration of H_2 is to compare its performance with the data reported in previous studies using the same pilot plant reactor under similar conditions and with the same sacrificial agent (methanol). In this way, Maldonado et al. [32] studied

Fig. 2. XRD of the fresh catalyst: Anatase (A), Rutile (R) and Tenorite (T).

photocatalytic H_2 production using a Cu/TiO_2 composite ($0.2\,g\,L^{-1}$), in presence of 0.05 M methanol at pH = 6–7, and they reported a maximum of $5.25\,\mu mol\,kJ^{-1}$ H_2 generation with the same pilot plant reactor. Also, the same reactor was used in a previous study of H_2 photogeneration based on Au/TiO_2 composite photocatalyst [16]. In that case when 0.05 M methanol was used as electron donor (with a catalyst load of $0.2\,g\,L^{-1}$) the maximum H_2 production was $5.0\,\mu mol\,kJ^{-1}$. With the data shown in Fig. 3 for methanol a H_2 production of $25.1\,\mu mol$ kJ^{-1} can be calculated. In consequence, the $CuO + TiO_2$ mixture studied here seems to produce 4–5 more H_2 than other more complex and expensive photocatalysts that have been widely studied as possible candidates for a real solar photocatalytic H_2 generation. Nevertheless, it has to be said that methanol was not the best choice of sacrificial agent for the Cu/TiO_2 and the Au/TiO_2 systems taken as references, and they could perform better with other sacrificial agents (see the energy efficiency assessment below). Although Au and Cu are co-catalyst prone to the scavenging of conduction band electrons and the suppression of electron-hole recombination, something that should, in principle, improve the hydrogen generation, the very simple $CuO + TiO_2$ mixture (with no stable and continuous contact between particles) shows a better performance. The excellent performance of this photocatalysts mixture can be tentatively explained by considering that it follows a Z-scheme charge transfer scheme. In this sense, when the $TiO_2 + CuO$ mixture is irradiated with solar light, photoexcited electrons are produced in both TiO_2 and CuO. TiO_2 absorbs only UV light because of the large band gap of ~ 3.2 eV, while CuO (~ 1.7 eV) absorbs both UV and visible light. Because the CB edge position of CuO is higher than NHE [36] the electrons produced in CuO can be used to reduce protons at the solid-electrolyte interphase and generate H_2. The CB electrons in the irradiated TiO_2 have lower energy than those in the CB of CuO [36] an suffer a transient accumulation until they are efficiently transferred to fill the VB holes of the CuO particle (distinctive Z-scheme charge transfer that is especially favored when the catalysts involved have different character, n-type for TiO_2 and p-type for CuO [36]). To complete the charge distribution picture, the holes formed at the TiO_2 move towards the particle surface and are transferred to the solution to produce the organic molecule oxidation. The color of the $TiO_2 + CuO$ slurry under irradiation became garnet-purple, this color change confirming the formation and accumulation of electrons at the TiO_2 CB before they are transferred to the CuO VB. The transient collision of CuO and TiO_2 particles allows the occurrence of the Z-scheme charge transfer mechanism, removing holes from CuO and electrons from TiO_2 and, thus, reducing intra-particle electron-hole recombination, and converting the $TiO_2 + CuO$ mixture in an effective photocatalyst combination for hydrogen production via water splitting.

Total organic carbon (TOC) of the solution decreased along H_2 formation (from 493 to $421\,mg\,L^{-1}$ after 6 h of irradiation with formic acid), a decrease that involves an excess of the number of electrons required for the observed H_2 generation. At the same time, temperature inside the reactor rose from 30 °C at the beginning of the experiments (9:30-10:00 a.m.) to approximately 50 °C (normally around 4:00 p.m.) although no clear relation between H_2 production rate and temperature was noticed.

The effect of pH on the photocatalytic reaction is shown in Fig. 4. As can be seen, the basic medium (pH = 9) offers the best condition for H_2 production, while acid conditions are clearly detrimental. At neutral pH an intermediate behavior is observed. The data shown in Fig. 4 was obtained by using glycerol as electron donor, and it is interesting to notice that the increase in pH leads to a hydrogen production similar to the one observed in Fig. 3 for formic acid.

This behavior of photocatalytic reactivity with pH has been already described in the photocatalytic generation of H_2 with a Pt/TiO_2 catalyst [37] and it might seem surprising because H_2 formation from water protons should, in principle, be favored at acid pH. There are several reasons that could explain the improvement of reaction rate of H_2 generation when changing from acid to neutral and basic pH. Those are
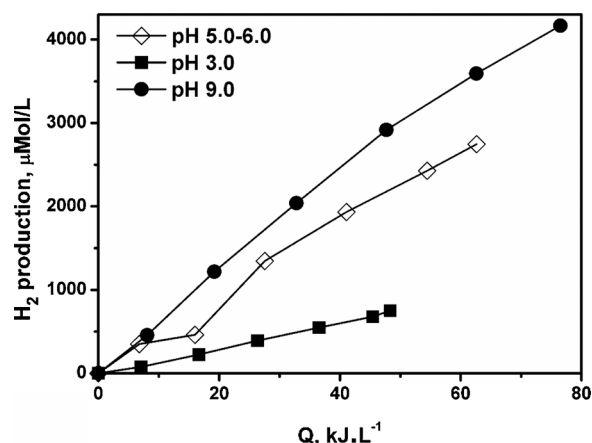

Fig. 4. Photocatalytic H_2 generation at different pH values by using glycerol as sacrificial electron donor. Glycerol = 0.05 M, $TiO_2 + CuO$ (10:1) $= 0.2\,g.L^{-1}$, V = 25 L, and total irradiation time of 6 h.

(a) the energy of the valence and conduction band levels of the semiconductor (that can change with pH) with respect to the redox potentials of the reacting redox couples in solution; (b) the dependence of the quantity and sign of the semiconductor surface electrical charge with pH, that influences the ability of the TiO_2 and CuO nanoparticles to approach and accomplish a Z-scheme charge transfer; (c) the speciation of electron donors in solution; and (d) the change of the size of photocatalyst particle aggregates with changing pH. Also, in the three experiments of Fig. 4 the initial pH decreased along the reaction (from 9.0, 5.9 and 3.0 to 5.5, 5.0 and 2.6 at the end of the process, respectively), suggesting that better H_2 production could have been obtained if pH had been keep controlled and constant at its initial value. The decrease of pH during the reaction can be probably due to the removal of H^+ from the solution, or to the release of important amounts of carboxylic acids generated during organic oxidation. From an applied point of view it is interesting to remark that neutral-slightly basic pH is the usual pH in natural waters and many wastewaters.

In order to check if an increase on H_2 generation occurs when the initial concentration of organic material in solution is higher, experiments were carried out with different dilutions of the original biodiesel industrial wastewater. Fig. 5 shows the evolution of H_2 when using 500, 1300 and $2500\,mg\,L^{-1}$ of initial TOC and, as can be seen, the change from 500 to $1300\,mg\,L^{-1}$ produces a dramatic improvement on H_2 generation, but the further increase to $2500\,mg\,L^{-1}$ turns out to be
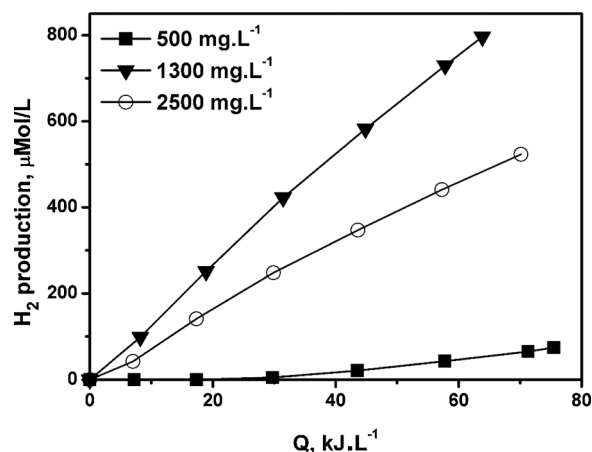

Fig. 5. Photocatalytic H_2 generation at different TOC concentrations by using a real biodiesel wastewater (see Table 1 for main chemical features) as a sacrificial agent. Reaction conditions: $TiO_2 + CuO$ (10:1) $= 0.2\,g.L^{-1}$, pH = 5.5–6.5, V = 25 L, and total irradiation time of 6 h.
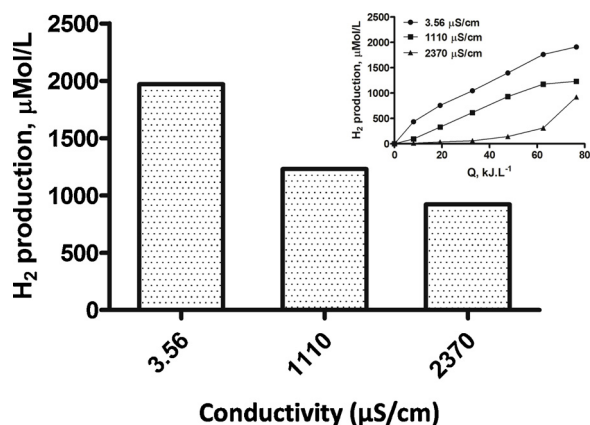
Fig. 6. Photocatalytic H_2 generation as a function of conductivity by using methanol as sacrificial agent. Reaction conditions: Methanol = 0.05 M, $TiO_2 + CuO$ (10:1) $= 0.2$ g.L^{-1}, pH = 5–6, V = 25 L, and total irradiation time of 6 h. Conductivities were obtained with different mixtures of demineralized and tap water (see Table 1 for main chemical features).

Fig. 7. H_2 generation in consecutive photocatalytic experiments using the same aqueous solution and the same sample of $TiO_2 + CuO$ (allowed to settle overnight and re-suspended during the day). Reaction conditions: Formic acid = 0.05 M, $TiO_2 + CuO$ (10:1) $= 0.2$ g.L^{-1}, pH = 2–3, V = 25 L.

detrimental. In consequence, an optimal organic content must exist above which the H_2 production decreases.

Two causes could account for this reduction of activity with a high organic content: a) the increase of the solution color that competes with the photocatalytic process for the capture of photons, and b) the existence of a high conductivity, because this is a real wastewater with more components that just glycerol, and in particular it is a water with an important salt content (solutions with high conductivities normally hamper photocatalytic processes [15,16,32]). Therefore, another set of experiments were designed to check the possible effect of electric conductivity on the photocatalytic efficiency of the CuO + TiO_2 mixture. In that case, solutions of methanol were prepared by dissolving this chemical in different mixtures of demineralized and tap water. Since the PSA tap water has a conductivity of 2500 µS cm^{-1}, the methanol solutions with different proportions of tap water had also different conductivities. Fig. 6 clearly shows that the increase on conductivity produces a dramatic decrease on photocatalytic activity, rendering a system that has little capacity for H_2 production.

Consequently, this should be the most likely cause of the decrease of photocatalytic activity when using more concentrated samples of the biodiesel wastewater because the conductivity of that wastewater moves from 130 to 900 µS cm^{-1} when changing from 500 to 2500 mg L^{-1} of TOC content. Thus, the content of inorganic salts or any other chemical feature that can increase the conductivity of the water used in this type of photocatalytic processes is one of the main limiting factors of the reaction efficiencies and they have to be carefully checked if a successful real application is envisaged. In fact, another industrial wastewater (a sample collected from the inlet of the municipal wastewater treatment plant of Almería) with a higher conductivity (around 2000 µS cm^{-1}) than biodiesel wastewater was also checked in this work with the CuO + TiO_2 mixture and no any H_2 production was observed.

On the other hand, although in all cases TOC decreases along the reaction, the total quantity of removal after 6 h reactions is rather discrete (no more than 80-50 mg L^{-1}). This arises the question whether this mixture of photocatalysts is able to efficiently remove large quantities of organics from water and produce a real cleaning of polluted wastewaters.

A long term experiment, consisting on the irradiation of the same sample of water and mixture of photocatalysts on consecutive days was carried out. At night, and in absence of light, the pumping of the slurry to the solar collector stopped and the catalyst powder was allowed to settle, and with the return of light the pumping resumed, and the powder was re-suspended. Fig. 7 shows the production of H_2 in the five consecutive days of the experiment that was carried out using a 0.05 M
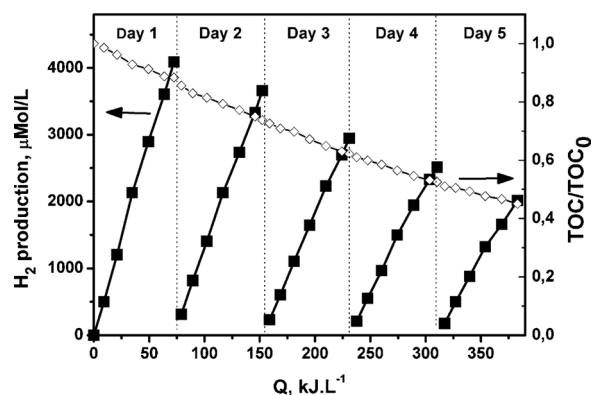
solution of formic acid at pH = 2-3.

Reactor irradiation times during the day oscillated from 340 to 390 min, corresponding to Q_n values that ranged from 72.5 to 79 kJ L^{-1}. As can be seen, a continuous decrease of TOC, with no remarkable discontinuities between consecutive days, is observed reaching more than 50% (570 to 257 mg L^{-1}) removal at the end of the fifth day. Moreover, the reduction of TOC detected during the first day (more than 70 mg L^{-1}) is the best one observed for all the aqueous organic compounds tested in this work, in agreement with the largest production of H_2 of the formic acid solutions. The system is also able to produce H_2 during the five days, although the 4091 µmol L^{-1} obtained at the end of the first day are reduced to 2014 µmol L^{-1} at the end of the five day. Also, a clear deposition of the catalyst on the inside walls of the CPC pyrex tubes takes place after repeated experiments. Although a drop in activity should be expected in agreement with the continuous decrease of the organic sacrificial agent and the corresponding decrease of reaction kinetics, extra attention has been paid to this experimental behavior in order to detect the existence of an alternative deactivation mechanism. In this sense, the observed partial deactivation of the photocatalysts when using formic acid solutions has been studied by characterizing the solid photocatalysts after 1 and 5 reaction cycles (1 and 5 days). The XRD powder patterns of the solids after 1 and 5 cycles (Figure S1) are similar to that of observed for the fresh catalyst (Fig. 2), but now the reflection lines due to tenorite CuO were not observed. This can be due to either the lost of the copper species (deposition on the pyrex walls), or to the formation of amorphous phases. Moreover, the surface of the photocatalysts was studied by XPS.

Fig. 8 shows the Cu $2p_{3/2}$ core level spectra for the fresh catalyst and after 1 and 5 cycles. Table 2 includes the XPS data of the C $1s$, O $1s$, Ti $2p_{3/2}$ and Cu $2p_{3/2}$ signals, and Table 3 the surface chemical composition determined by XPS. The Cu $2p_{3/2}$ core level spectrum of the fresh catalysts shows two contributions to the main peak at 932.3 and 934.2 eV assigned to reduced copper, probably as Cu^{1+}, and Cu^{2+} from tenorite, respectively [38], and the corresponding shake-up satellites at 940.1 and 943.2 eV of Cu^{2+}.

The frequently useful Auger Cu LMM signal was recorded, but in this case it was of no use because it overlapped with the Ti $2s$ signal. The % of surface Cu^{2+} was calculated taking into account the area contributions of the main peak at 934.2 eV and the corresponding shake-up satellites. After 1 cycle, the Cu $2p_{3/2}$ core level spectrum (see Fig. 8) shows modifications. The relative intensity of the contribution at low binding energy (932.4 eV), due to reduced copper species, increases and the % of Cu^{2+} decreases from 58 to 43%. Clearly, the photocatalytic process produces a reduction of Cu^{2+}, although the atomic concentration of Cu is almost constant after the 1 st cycle (Table 3).
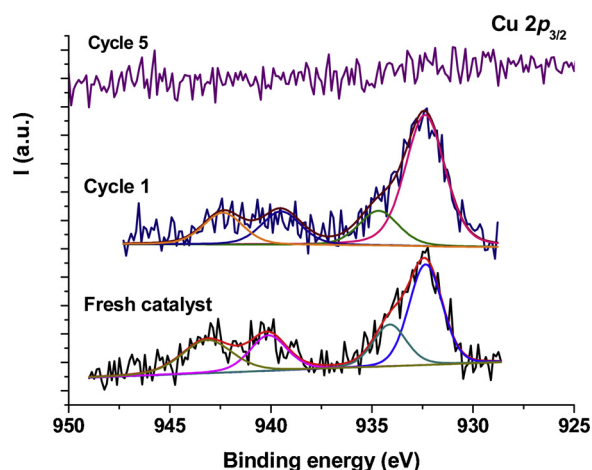
Fig. 8. Cu $2p_{3/2}$ core level spectra for the fresh catalyst, and after 1 and 5 cycles in presence of formic acid.

Fig. 9. UV–vis-NIR Diffuse reflectance spectra of the studied catalysts.

Table 2
Binding energy values for the studied catalysts, and % of Cu^{2+}.

Sample	C 1s	O 1s	Ti $2p_{3/2}$	Cu $2p_{3/2}$	%Cu^{2+}
Fresh catalyst	284.8 85%	529.8 90%	458.6	932.3	58
	286.3 7%	531.0 7%		934.2	
	288.7 8%	531.9 3%			
Cycle 1	284.8 88%	529.8 88%	458.5	932.4	43
	286.1 4%	530.7 7%		934.7	
	288.7 8%	531.7 5%			
Cycle 5	284.8 85%	529.8 86%	458.7	n.d.	
	286.1 8%	530.9 8%			
	288.7 7%	531.8 6%			

Table 3
Surface composition in atomic % determined by XPS.

Sample	C 1s	O 1s	Ti 2p	Cu 2p
Fresh catalyst	24.71	53.15	21.33	0.81
Cycle 1	23.60	53.53	21.98	0.80
Cycle 2	21.06	57.30	21.64	n.d.

Thus, this seems to indicate that a net loss of Cu (both, Cu^+ and Cu^{2+}) is taking place during the process. Indeed, after 5 cycles, no presence of Cu is observed in the photocatalyst surface.

On the other hand, the C 1s core level spectra of the three samples are very similar. They can be decomposed in three contributions (Table 2). The more intense at 284.8 eV is assigned to adventitious carbon, the second one at about 286.1 eV is due to C−OH and C−O−C bonds, and the third one at 288.7 eV is due to carbonate. The presence of surface carbonate is typically observed when copper is used as surface catalyst in organic oxidation processes [39], although in this case it could also be assigned to formic acid adsorption. However, the fact that elemental analysis of the samples (Table 4) shows a clear increase of C and H content when comparing the fresh catalyst sample and the solid recovered after cycle 5 seems to indicate that formic acid adsorption is rather low and the C 1s XPS signal associated to carbonate is due to reaction products.

Table 4
C,H,N elemental analysis.

Sample	%C	%H	%N
Fresh catalyst	0.136	0.000	0.000
Cycle 1	0.218	0.019	0.000
Cycle 2	0.504	0.043	0.020

The Ti $2p_{3/2}$ signal appears at about 458.6 eV, typical of Ti^{4+} in the TiO_2 phase. The O 1s core level signals are decomposed in three contributions (see Table 2), being the more intense at about 529.8 eV assigned to lattice oxygen of TiO_2 and CuO [40], while that observed at high binding energy (531.7 eV) can be associated to surface carbonates.

The UV–vis-NIR diffuse reflectance spectra of the support P25, fresh catalyst and of the catalysts after 5 cycles are shown in Fig. 9, while Fig. 10 displays the corresponding Taue plots. The Vis-NIR region of the diffuse reflectance spectrum of the fresh catalyst is very similar to that reported for CuO nanoflakes, and typical of Cu^{2+} [41]. The calculated band gap value for P25 is 3.27 eV (Fig. 9), while the fresh catalyst with CuO shows a band gap of 1.7 eV, more or less similar to that of CuO tenorite [42]. After 5 cycles, the spectrum is similar to that of P25, showing a band gap of 3.17 eV, and indicating the absence of CuO. To complete the characterization, the chemical composition was also studied by XRF and, as shown in Table 5, after 5 cycles the sample does not contain copper, thus supporting the fact that Cu is leaching along the photocatalytic process.

The fact that a large production of H_2 is taken place even at the end of the fifth cycle when very little CuO is detected can only be explained by considering that CuO do not leave the reactor but it remains on the CPC pyrex walls, and can continue to do its role.

Finally, a quantitative assessment of the capacity of the CuO + TiO_2 mixtures to convert solar to chemical energy is carried out. This assessment will also help to compare in a more fair way the capacity of H_2 production of this system with previously reported ones. The solar to hydrogen energy conversion factor (STH, amount of chemical energy stored in the produced H_2 vs. amount of solar energy accumulated in the CPC reactor) was calculated by using the following equation [43]:

$$\eta = \frac{\Delta G_{H_2}^0 \Delta H_2 V_g}{Q \cdot V_L} 100\% \qquad (3)$$

where $\Delta G_{H_2}^0$ is the Gibbs free energy of a H_2 molecule (283.6 kJ mol^{-1}), ΔH_2 is the quantity of hydrogen produced in a lapse of reaction time (in mol·L^{-1}), Q is the energy entering the photoreactor during the same lapse of time (in kJ·L^{-1}, and only taking into account wavelengths below 400 nm), and V_g and V_L are the volume of the gas headspace and illuminated liquid phase of the reactor, respectively. The experiment chosen for the calculation is the one using formic acid in Fig. 7 (day 1) because it corresponds to the best H_2 production shown in this work, with 67.3 kJ L^{-1} of energy generating 4123 μmol·L^{-1} of H_2.

By using Eq. (3) an STH of 2.6% is obtained. Although solar light involves both visible and UV light, this can be considered an interesting result because the maximum efficiencies reported so far for H_2 generation using visible light are around 5% [44], but particularly because the mixture of commercially available CuO + TiO_2 is an extremely
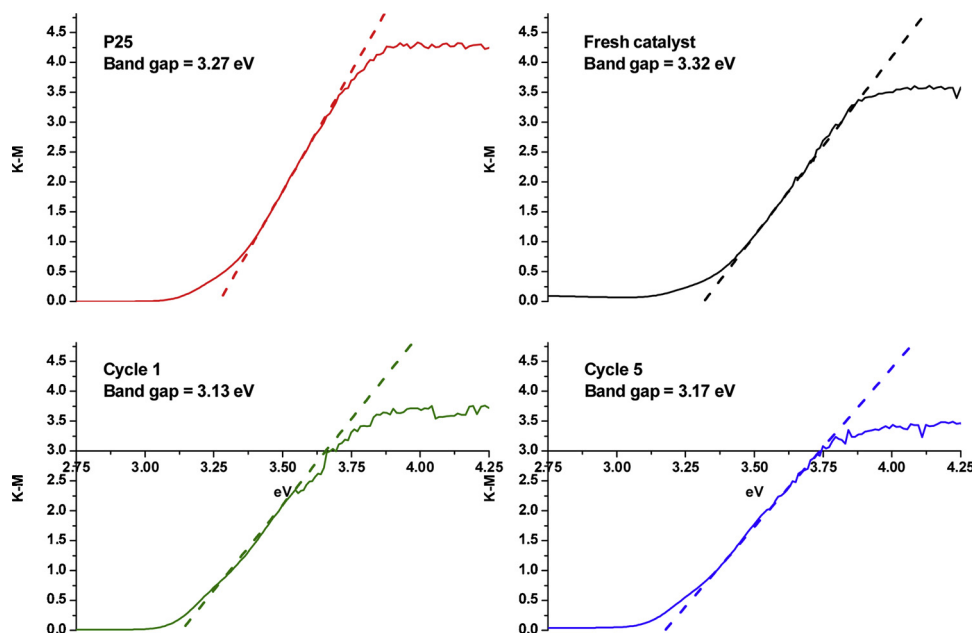
Fig. 10. Taue plots of the studied catalysts and commercial P25 sample.

Table 5
Chemical composition in wt.% of the fresh catalysts and the material after 5 cycles determined by XRF.

	Fresh Catalyst	Cycle 5
TiO_2	91.20	99.14
CuO	8.32	0.01

simple, and very cheap system that needs no previous steps of composite preparation and involve no scarce and expensive materials. For the sake of comparison, other more complex and expensive photocatalytic systems that were tested in the same pilot plant produced similar or less H_2: 2.5% and 1.6% STH for a Pt/(TiO_2-N) (a N doped TiO_2 with Pt deposits) and a Pt/(CdS-ZnS) photocatalysts, respectively [15], 2.9% with a Au/TiO_2 photocatalyst [16], and 2.6% with a Cu/TiO_2 [32]. Thus, the simple Cu + TiO_2 mixture is able to produce similar amounts of photocatalytic H_2 than expensive composites like Pt/(TiO_2-N) or Au/TiO_2.

4. Conclusions

The need for a cheap and green H_2 production has led to the search of cheap and simple photocatalytic materials that can convert solar energy into chemical energy. In this sense, a mixture of commercially available CuO and TiO_2 irradiated in presence of organic sacrificial agents has shown similar H_2 productions to the ones obtained with more complex materials like Au/TiO_2, Pt/(TiO_2-N), or Cu/TiO_2. A solar driven pilot plant scale photocatalytic reactor has been used to test the mixture of catalysts performance, and different compounds like methanol, glycerol, formic acid, and the organic content of a biodiesel industry wastewater have played the role of sacrificial electron donors. Formic acid solutions have provided the best hydrogen production. For the rest of electron donors neutral or basic pH values have been better than acid ones. The fact that glycerol and a real wastewater coming from the biodiesel industry that contains high quantities of glycerol, are able to sustain remarkable productions of hydrogen is very interesting because large quantities of those wastewaters are generated annually worldwide. The system also removes more than 50% of the original TOC content along consecutive days of irradiation with sustained generation of hydrogen. Finally, a clear reduction of the Cu content has

been detected by characterizing the sample obtained after 5 consecutive runs, a process that is in agreement with the deposition of the catalyst on the walls of the CPC reactor.

Appendix A. Supplementary data

Supplementary material related to this article can be found, in the online version, at doi:https://doi.org/10.1016/j.apcatb.2019.117890.

References

[1] A. Kubacka, M. Fernández-García, G. Colón, Advanced nanoarchitectures for solar photocatalytic applications, Chem. Rev. 112 (2012) 1555–1614, https://doi.org/10.1021/cr100454n.

[2] G. Zhang, X. Wan, A wind-hydrogen energy storage system model for massive wind energy curtailment, Int. J. Hydrogen Energy 39 (2014) 1243–1252, https://doi.org/10.1016/j.ijhydene.2013.11.003.

[3] T.N. Vezirolu, F. Barbir, Hydrogen: the wonder fuel, Int. J. Hydrogen Energy 17 (1992) 391–404, https://doi.org/10.1016/0360-3199(92)90183-W.

[4] O. Bičáková, P. Straka, Production of hydrogen from renewable resources and its effectiveness, Int. J. Hydrogen Energy 37 (2012) 11563–11578, https://doi.org/10.1016/j.ijhydene.2012.05.047.

[5] A. Fujishima, K. Honda, Electrochemical photolysis of water at a semiconductor electrode, Nature 238 (1972) 37–38, https://doi.org/10.1038/238037a0.

[6] A. Fujishima, X. Zhang, D.A. Tryk, Heterogeneous photocatalysis: from water photolysis to applications in environmental cleanup, Int. J. Hydrogen Energy 32 (2007) 2664–2672, https://doi.org/10.1016/j.ijhydene.2006.09.009.

[7] S.W. Bae, S.M. Ji, S.J. Hong, J.W. Jang, J.S. Lee, Photocatalytic overall water splitting with dual-bed system under visible light irradiation, Int. J. Hydrogen Energy 34 (2009) 3243–3249, https://doi.org/10.1016/j.ijhydene.2009.02.022.

[8] A. Kudo, Y. Miseki, Heterogeneous photocatalyst materials for water splitting, Chem. Soc. Rev. 38 (2009) 253–278, https://doi.org/10.1039/B800489G.

[9] G. Colón, Towards the hydrogen production by photocatalysis, Appl. Catal. A Gen. 518 (2016) 48–59, https://doi.org/10.1016/j.apcata.2015.11.042.

[10] M.S. Park, M. Kang, The preparation of the anatase and rutile forms of Ag-TiO2 and hydrogen production from methanol/water decomposition, Mater. Lett. 62 (2008) 183–187, https://doi.org/10.1016/j.matlet.2007.04.105.

[11] A. Patsoura, D.I. Kondarides, X.E. Verykios, Photocatalytic degradation of organic pollutants with simultaneous production of hydrogen, Catal. Today 124 (2007)

94–102, https://doi.org/10.1016/j.cattod.2007.03.028.

[12] J. Wang, P. Yang, B. Cao, J. Zhao, Z. Zhu, Photocatalytic carbon-carbon bond formation with concurrent hydrogen evolution on the Pt/TiO2 nanotube, Appl. Surf. Sci. 325 (2015) 86–90, https://doi.org/10.1016/j.apsusc.2014.10.143.

[13] Y. Xu, R. Xu, Nickel-based cocatalysts for photocatalytic hydrogen production, Appl. Surf. Sci. 351 (2015) 779–793, https://doi.org/10.1016/j.apsusc.2015.05.171.

[14] S. Xu, A.J. Du, J. Liu, J. Ng, D.D. Sun, Highly efficient CuO incorporated TiO2 nanotube photocatalyst for hydrogen production from water, Int. J. Hydrogen Energy 36 (2011) 6560–6568, https://doi.org/10.1016/j.ijhydene.2011.02.103.

[15] K. Villa, X. Domènech, S. Malato, M.I. Maldonado, J. Peral, Heterogeneous photocatalytic hydrogen generation in a solar pilot plant, Int. J. Hydrogen Energy (2013) 12718–12724, https://doi.org/10.1016/j.ijhydene.2013.07.046.

[16] S.Y. Arzate Salgado, R.M. Ramirez Zamora, R. Zanella, J. Peral, S. Malato, M.I. Maldonado, Photocatalytic hydrogen production in a solar pilot plant using a Au/TiO2 photo catalyst, Int. J. Hydrogen Energy 41 (2016) 11933–11940, https://doi.org/10.1016/j.ijhydene.2016.05.039.

[17] R. Dholam, N. Patel, M. Adami, A. Miotello, Physically and chemically synthesized TiO2 composite thin films for hydrogen production by photocatalytic water splitting, Int. J. Hydrogen Energy 33 (2008) 6896–6903, https://doi.org/10.1016/j.ijhydene.2008.08.061.

[18] F. Xu, W. Xiao, B. Cheng, J. Yu, Direct Z-scheme anatase/rutile bi-phase nanocomposite TiO2 nanofiber photocatalyst with enhanced photocatalytic H2-production activity, Int. J. Hydrogen Energy 39 (2014) 15394–15402, https://doi.org/10.1016/j.ijhydene.2014.07.166.

[19] S. Yang, H. Wang, H. Yu, S. Zhang, Y. Fang, S. Zhang, F. Peng, A facile fabrication of hierarchical Ag nanoparticles-decorated N-TiO2 with enhanced photocatalytic hydrogen production under solar light, Int. J. Hydrogen Energy 41 (2016) 3446–3455, https://doi.org/10.1016/j.ijhydene.2015.12.190.

[20] D.Y.C. Leung, X. Fu, C. Wang, M. Ni, M.K.H. Leung, X. Wang, X. Fu, Hydrogen production over Titania-based photocatalysts, ChemSusChem 3 (2010) 681–694, https://doi.org/10.1002/cssc.201000014.

[21] S. Xu, D.D. Sun, Significant improvement of photocatalytic hydrogen generation rate over TiO2 with deposited CuO, Int. J. Hydrogen Energy 34 (2009) 6096–6104, https://doi.org/10.1016/j.ijhydene.2009.05.119.

[22] W. Chen, V. Jovic, D. Sun-Waterhouse, H. Idriss, G.I.N. Waterhouse, The role of CuO in promoting photocatalytic hydrogen production over CuO/TiO2, Int. J. Hydrogen Energy 38 (2013) 15036–15048, https://doi.org/10.1016/j.ijhydene.2013.09.101.

[23] J.M. Kum, S.H. Yoo, G. Ali, S.O. Cho, Photocatalytic hydrogen production over CuO and TiO2 nanoparticles mixture, Int. J. Hydrogen Energy 38 (2013) 13541–13546, https://doi.org/10.1016/j.ijhydene.2013.08.004.

[24] Y.H. Yu, Y.P. Chen, Z. Cheng, Microwave-assisted synthesis of rod-like CuO/TiO2 for high-efficiency photocatalytic hydrogen evolution, Int. J. Hydrogen Energy 40 (2015) 15994–16000, https://doi.org/10.1016/j.ijhydene.2015.09.115.

[25] A. Petala, E. Ioannidou, A. Georgaka, K. Bourikas, D.I. Kondarides, Hysteresis phenomena and rate fluctuations under conditions of glycerol photo-reforming reaction over CuOx/TiO2 catalysts, Appl. Catal B: Environ. 178 (2015) 201–209, https://doi.org/10.1016/j.apcatb.2014.09.021.

[26] A. Kubacka, M.J. Muñoz-Batista, M. Fernández-García, S. Obregón, G. Colón, Evolution of H2 photoproduction with Cu content on CuOx-TiO2 composite catalysts prepared by a microemulsion method, Appl. Catal. B: Environ. 163 (2015) 214–222, https://doi.org/10.1016/j.apcatb.2014.08.005.

[27] B.A. Pinaud, J.D. Benck, L.C. Seitz, A.J. Forman, Z. Chen, T.G. Deutsch, B.D. James, K.N. Baum, G.N. Baum, S. Ardo, H. Wang, E. Miller, T.F. Jaramillo, Technical and economic feasibility of centralized facilities for solar hydrogen production via photocatalysis and photoelectrochemistry, Energy Environ. Sci. 6 (2013) 1983, https://doi.org/10.1039/c3ee40831k.

[28] C.A. Rodriguez, M.A. Modestino, D. Psaltis, C. Moser, Design and cost

considerations for practical solar-hydrogen generators, Energy Environ. Sci. 7 (2014) 3828–3835, https://doi.org/10.1039/C4EE01453G.

[29] E. Baniasadi, I. Dincer, G.F. Naterer, Exergy and environmental impact assessment of solar photoreactors for catalytic hydrogen production, Chem. Eng. J. 213 (2012) 330–337, https://doi.org/10.1016/j.cej.2012.10.018.

[30] C.A. Linkous, N.Z. Muradov, S.N. Ramser, Consideration of reactor design for solar hydrogen production from hydrogen sulfide using semiconductor particulates, Int. J. Hydrogen Energy 20 (1995) 701–709, https://doi.org/10.1016/0360-3199(94)00127-L.

[31] D. Jing, H. Liu, X. Zhang, L. Zhao, L. Guo, Photocatalytic hydrogen production under direct solar light in a CPC based solar reactor: reactor design and preliminary results, Energy Convers. Manage. 50 (2009) 2919–2926, https://doi.org/10.1016/j.enconman.2009.07.012.

[32] M.I. Maldonado, A. López-Martín, G. Colón, J. Peral, J.I. Martínez-Costa, S. Malato, Solar pilot plant scale hydrogen generation by irradiation of Cu/TiO2 composites in presence of sacrificial electron donors, Appl. Catal. B: Environ. 229 (2018) 15–23, https://doi.org/10.1016/j.apcatb.2018.02.005.

[33] S. Malato, P. Fernández-Ibáñez, M.I. Maldonado, J. Blanco, W. Gernjak, Decontamination and disinfection of water by solar photocatalysis: recent overview and trends, Catal. Today 147 (2009) 1–59, https://doi.org/10.1016/j.cattod.2009.06.018.

[34] W.C. Lin, W.D. Yang, I.L. Huang, T.S. Wu, Z.J. Chung, Hydrogen production from methanol/water photocatalytic decomposition using Pt/TiO2-xNx catalyst, Energy Fuels 23 (2009) 2192–2196, https://doi.org/10.1021/ef801091p.

[35] J. Colina-Márquez, F. MacHuca-Martínez, G.L. Puma, Radiation absorption and optimization of solar photocatalytic reactors for environmental applications, Environ. Sci. Technol. 44 (2010) 5112–5120, https://doi.org/10.1021/es100130h.

[36] M. Janczarek, E. Kowalska, On the origin of enhanced photocatalytic activity of copper-modified Titania in the oxidative reaction systems, Catalysts 7 (2017) 317–343, https://doi.org/10.3390/catal7110317.

[37] V.M. Daskalaki, D.I. Kondarides, Efficient production of hydrogen by photo-induced reforming of glycerol at ambient conditions, Catal. Today 144 (2009) 75–80, https://doi.org/10.1016/j.cattod.2008.11.009.

[38] E. Moretti, L. Storaro, A. Talon, P. Riello, A. Infantes Molina, E. Rodriguez-Castellon, 3-D flower like Ce–Zr–Cu mixed oxide systems in the CO preferential oxidation (CO-PROX): Effect of catalyst composition, Appl. Catal. B: Environ. 168-169 (2015) 385–395.

[39] W.N.W. Isahak, Z.A.C. Ramli, M.W. Ismail, K. Ismail, R.M. Yusop, M.W.M. Hisham, M.A. Yarmo, Adsorption–desorption of CO2 on different type of copper oxides surfaces:Physical and chemical attractions studies, J. CO2 Util. 2 (2013) 8–15.

[40] J.F. Moulder, W.F. Stickle, P.E. Sobol, K.D. Bomben, J. Chastain (Ed.), Handbook of X-Ray Photoelectron Spectroscopy, Perkin-Elmer Corporation, Eden Prairie, MN, 1992.

[41] H. Siddiqui, M.S. Qureshi, F.Z. Haque, Valuation of copper oxide (CuO) nanoflakes for its suitability as an absorbing material in solar cells fabrication, Optik 127 (2016) 3713–3717.

[42] C.E. Ekuma, V.I. Anisimov, J. Moreno, M. Jarrell, Electronic structure and spectra of CuO, Eur. Phys. J. B 87 (2014) 40949–40955.

[43] Q. Wang, T. Hisatomi, Q. Jia, H. Tokudome, M. Zhong, C. Wang, Z. Pan, T. Takata, M. Nakabayashi, N. Shibata, Y. Li, I.D. Sharp, A. Kudo, T. Yamada, K. Domen, Scalable water splitting on particulate photocatalyst sheets with a solar-to-hydrogen energy conversion efficiency exceeding 1%, Nat. Mater. 15 (2016) 611–615, https://doi.org/10.1038/nmat4589.

[44] K. Maeda, K. Teramura, K. Domen, Effect of post-calcination on photocatalytic activity of (Ga1-xZnx)(N1-xOx) solid solution for overall water splitting under visible light, J. Catal. 254 (2008) 198–204, https://doi.org/10.1016/j.jcat.2007.12.009.